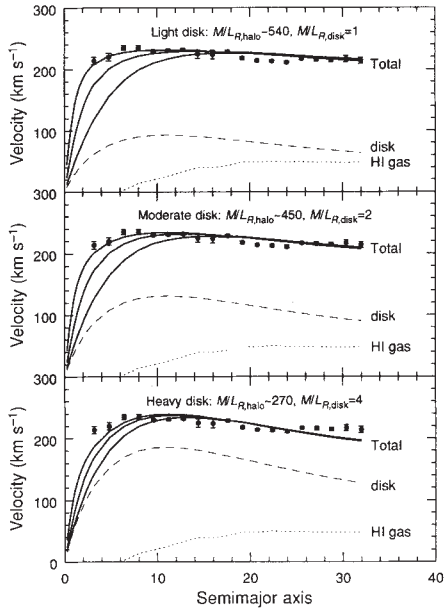

FIG. 3 The rotation curve of the galaxy NGC5907 as derived from observations of the 21-cm line of neutral hydrogen[2] is shown with model curves. In each panel, the dotted line shows the curve that would be expected from the H I gas alone and the dashed line indicates the rotation curve of the thin exponential disk alone. The thick solid lines are the complete rotation curves, namely the quadrature sum of the gas curve, disk curve, and the rotation curve of haloes producing similarly good fits to the light: an $r^{-2.22}$ halo, with $c/a=0.51$ and a 1-kpc core (top curve); an $r^{-2.26}$ halo, with $c/a=0.53$ and a 2-kpc core (middle curve; R-band residuals shown in Fig. 2*d*); and an $r^{-2.74}$ halo, with $c/a=0.53$ and a 6-kpc core (bottom curve). The central dark mass densities of these models are 1.9, 0.45 and 0.08 $M_\odot$ pc^{-3} respectively. In the middle panel, the mass of the disk is assumed to be 5.3×10^{10} $M_\odot$, derived using $M/L_R=2$ (appropriate to Sc galaxies) and a luminosity based on the Tully–Fisher relation. The M/L_R of the halo component has been scaled to give a good fit to the rotation curve: $M/L_R=420$ for the $r^{-2.22}$ halo, $M/L_R=450$ for the $r^{-2.26}$ halo, and $M/L_R=455$ for the $r^{-2.74}$ halo. Plausible fits to the curve can be obtained with plausible $1\lesssim M/L_{R,disk}\lesssim4$ (top, middle and bottom panels) for an Sc disk, resulting in $270\lesssim M/L_{R,halo}\lesssim540$ for the halo, though the high $M/L_{R,disk}$ and low $M/L_{R,halo}$ give notably poorer fits. (All M/L are given in solar units.) The $r^{-3.5}$ distribution cannot provide the required rotation support beyond the edge of the stellar disk (~20 kpc). The rotation curve inward of 5 kpc is affected by light inside our mask and by the small bulge component seen in the infrared[10].

As halo stars have high space motions, proper-motion surveys provide one of the best constraints on the existence of a massive halo of M subdwarfs in our own Milky Way. Assuming kinematics similar to the Galaxy's Population II halo, the numbers of M subdwarfs in one such proper-motion catalogue[27] fall short by at least an order of magnitude (C. C. Dahn, J. Liebert, H. C. Harris, P. C. Boeshaar, manuscript in preparation), suggesting that the Galaxy's massive halo is not composed of such objects. Deep pencil-beam surveys of the Milky Way capable of accurate star–galaxy separation at $V=26$ mag or fainter would also place tight constraints on a dark-matter halo of late M subdwarfs in the Galaxy, because such surveys would probe distances up to 2 kpc and thus detect ~20 of these faint halo stars per square arcmin.

For external galaxies, the decisive observations, which are in reach of current technology, will be surface-brightness measurements in the V and I bands. If the stellar population emitting the faint halo light of NGC5907 is similar to that of known population II stars, its $(V-I)$ colour should be ~1.0 (ref. 28); observed late M dwarfs have $(V-I)$ colours near 2.5 (ref. 22). □

Received 22 April; accepted 28 June 1994.

1. Ashman, K. M. *Proc. astr. Soc. Pacif.* **104,** 1109–1138 (1992).
2. Sancisi, R. & van Albada, T. S. in *Int. Astr. Un. Symp. No. 117* (eds Kormendy, J. & Knapp, G. R.) 67–81 (Reidel, Dordrecht, 1987).
3. Morrison, H. L., Boroson, T. A. & Harding, P. *Astr. J.* (in the press).
4. Tyson, J. A. *Astr. J.* **96,** 1–23 (1988).
5. Caldwell, N., Armandoff, T. E., Seitzer, P. & Da Costa, G. D. *Astr. J.* **103,** 840–850 (1992).
6. Freeman, K. C. *A. Rev. Astr. Astrophys.* **25,** 603–632 (1987).
7. Zinn, R. *Astrophys. J.* **293,** 424–444 (1985).
8. Pritchet, C. J. & van den Burgh, S. *Astr. J.* **107,** 1730–1736 (1994).
9. Kormendy, J. & Bruzal, A. G. *Astrophys. J.* **223,** L63–L66 (1978).
10. Barnaby, D. & Thronson, H. A. *Astr. J.* **107,** 1717–1729 (1994).
11. Morrison, H. L. *Astr. J.* **106,** 578–590 (1993).
12. Harris, H. G., Bothun, G. D. & Hesser, J. E. in *Int. Astr. Un. Symp. No. 126* (eds Grindlay, J. E. & Davis Philip, A. G. 613–614 (Reidel, Dordrecht, 1988).
13. Bahcall, N. A. *A. Rev. Astr. Astrophys.* **15,** 505–540 (1977).
14. Gott, J. R. *A. Rev. Astr. Astrophys.* **15,** 235–266 (1977).
15. Lake, G. & Feinswog, L. *Astr. J.* **98,** 166–179 (1989).
16. Broeils, A. thesis, Univ. Groningen (1992).
17. Buchhorn, M. thesis, Australian natn. Univ. (1992).
18. Sackett, P. D., Rix, H.-W., Jarvis, B. J. & Freeman, K. C. *Astrophys. J.* (in the press).
19. Alcock, C. *et al. Nature* **365,** 621–623 (1993).
20. Aubourg, E. *et al. Nature* **365,** 623–625 (1993).
21. Udalski, A. *et al. Acta astr.* **43,** 289–294 (1993).
22. Monet, D. G. *et al. Astr. J.* **103,** 638–665 (1992).
23. Saumon, D., Bergeron, P., Lunine, J. I., Hubbard, W. B. & Burrows, A. *Astrophys. J.* **424,** 333–344 (1994).
24. Burrows, A., Hubbard, W. B. & Lunine, J. I. in *Proc. 8th Cambridge Workshop on Cool Stars, Stellar Systems, and the Sun (Publs astr. Soc. Pacif.)* (in the press).
25. van der Kruit in *Int. Astr. Un. Symp. No. 117* (eds Kormendy, J. & Knapp, G. R.) 415–424 (Reidel, Dordrecht, 1987).
26. Skrutskie, M. F., Shure, M. A. & Beckwith, S. *Astrophys. J.* **299,** 303–311 (1985).
27. Luyten, W. J. *Publs. Catalogue* (Univ. Minnesota Press, Minneapolis, 1979).
28. Reed, C. B. *Publs astr. Soc. Pacif.* **97,** 120–125 (1985).

ACKNOWLEDGEMENTS. We are grateful to R. Sancisi for supplying the H I rotation curve of NGC5907, and A. Burrows and J. Liebert for illuminating discussions about low-mass stars. We thank H.-W. Rix for for acting as scientific matchmaker and K. Freeman and L. Searle for suggestions that improved the presentation of this paper. P.D.S. is a J. Seward Johnson Fellow at the Institute for Advanced Study; H.L.M. is a Hubble Fellow at the National Optical Astronomy Observatory.

Interstellar oxide grains from the Tieschitz ordinary chondrite

L. R. Nittler, C. M. O'D Alexander, X. Gao, R. M. Walker & E. K. Zinner

McDonnell Center for the Space Sciences and Department of Physics, Washington University, One Brookings Drive, St. Louis, Missouri, 63130-4899, USA

MOST material in the Solar System has an isotopic composition that represents an average of the different stars that contributed material to the protostellar cloud. Primitive meteorites, on the other hand, preserve grains that retain the isotopic signatures of their individual stellar sources[1] and thus provide valuable insight into stellar and galactic evolution, nucleosynthesis, and solar nebular processes. A large number of pre-solar silicon carbide, graphite and diamond grains have now been isolated[1,2], but only three interstellar oxide grains have hitherto been recovered[3–7], even though oxygen-rich stars are believed to be the dominant source of dust in the Galaxy[8,9]. We report here the isolation of 21 interstellar oxide grains from the Tieschitz meteorite. The grains exhibit a wide range of oxygen isotope compositions, indicating that they originated in several distinct stellar sources having different masses and initial compositions. There is also evidence for the presence of the short-lived radionuclide ^{26}Al in nine of the grains at the time they formed. Although the isotopic compositions of many of the grains are consistent with both observations and theoretical models of oxygen-rich red giant stars, a significant fraction have no observed stellar counterpart.

Different isotopes are produced by a variety of nucleosynthetic processes, and the isotopic ratios in interstellar grains can therefore provide insight into the types of stellar sites that produced them. Here we determine the isotopic compositions of 21 inter-

stellar oxide grains isolated from the Tieschitz meteorite, and compare these values to astronomical observations and theoretical models of stellar evolution.

A sample of the Tieschitz (H/L 3.6) ordinary chondrite was physically and chemically processed to produce a residue[10,11], T8, in which chemically-resistant oxide phases were concentrated by a factor of $\sim 2.5 \times 10^5$. For ion microprobe analysis, a suspension of T8 was deposited on a gold foil[12] along with grains of the Burma Spinel oxygen isotope standard. To automatically locate rare interstellar oxides, a Photometrics CCD (charge-coupled device) camera was coupled to the microchannel plate/fluorescent screen of the modified Cameca IMS-3F ion microprobe[4] at Washington University. Low-mass-resolution ion images (in $^{16}O^-$ and $^{18}O^-$) of oxide grains were digitized, and the $^{16}O/^{18}O$ ratios ($\sigma \approx 4\%$) of individual grains were determined by image processing. Grains that deviated in duplicate analyses by more than 3σ from the solar $^{16}O/^{18}O$ ratio were selected for high-mass-resolution analysis. The high mass-resolving power needed to separate $^{16}OH^-$ ions from the $^{17}O^-$ ions precludes measurement of $^{16}O/^{17}O$ ratios by ion imaging in our instrument.

Ion imaging of ~6,000 grains yielded 53 candidates, the $^{16}O/^{18}O$ and $^{16}O/^{17}O$ ratios of which were subsequently measured at high mass resolution. Of these grains, 20 corundum (Al_2O_3) and 1 spinel ($MgAl_2O_4$) have a large range of anomalous (non-solar) $^{16}O/^{18}O$ and $^{16}O/^{17}O$ ratios (Fig. 1 and Table 1). Nine of the grains also have large ^{26}Mg excesses, corresponding to initial $^{26}Al/^{27}Al$ ratios of between 1.2×10^{-4} and 7.8×10^{-3}, much higher than the maximim value of 5×10^{-5} observed in primitive Solar System material (Fig. 2 and Table 1). All grains are 0.5–2 μm in size. For purposes of discussion, the 24 interstellar oxide grains found to date were divided into three groups on the basis of their oxygen isotope compositions (Fig. 1 and Table 1). Note that the range of oxygen isotope ratios usually observed in meteorites and terrestrial samples falls within the solar symbol in Fig. 1.

Group 1 grains have significant enrichments in ^{17}O and modest depletions in ^{18}O, similar to the isotopic compositions measured in O-rich red giants[13,14] (Table 1 and Fig. 1). These stars are thought to produce 65–75% of all dust, or ~80–90% of O-rich dust, in the Galaxy[8,9]. Because of this similarity, Group 1 grains probably formed in the atmospheres of red giants. The oxygen isotope compositions of such stars have been successfully reproduced by theoretical models in terms of the so-called first dredge-up, which occurs after exhaustion of H in the stellar core[15–18]. In this process, material that has undergone partial core H-burning via the CNO-cycle is mixed into the envelope. These models predict that the first dredge-up significantly decreases the envelope's initial $^{16}O/^{17}O$ ratio, the actual values depending primarily on stellar mass[16–18] (see Fig. 1). But the first dredge-up has only a relatively small effect on the $^{16}O/^{18}O$ ratio (20–50% increase), and larger differences in this ratio must be due to differences in the initial isotopic compositions of different stars[17] (Fig. 1). Such differences are the result of Galactic chemical evolution, reflecting age differences of the stars and/or the spread in chemical compositions observed in newly formed stars within a given Galactic epoch[19]. The range of the oxygen isotope compositions observed in the Group 1 grains indicates that they originated from several distinct stellar sources with different masses as well as different initial compositions.

As red giant stars continue to evolve, they can undergo two additional dredge-up episodes[15]. The second dredge-up occurs only in $>5M_\odot$ stars at the beginning of the asymptotic giant branch (AGB) phase, when He is exhausted in the star's core. The third dredge-up, which is experienced by all stars in the 1–$8M_\odot$ range, occurs during the thermally pulsing (TP) AGB phase when H and He burn alternately in thin shells on top of an inert core consisting now of C and O. These mixing episodes are not expected to significantly change the oxygen isotope composition of the envelope, although some spectroscopic observations of TP-AGB stars suggest that their atmospheres have higher $^{16}O/^{18}O$ and $^{16}O/^{17}O$ ratios than pre-TP-AGB stars[13,14,20,21] (Fig. 1*a*).

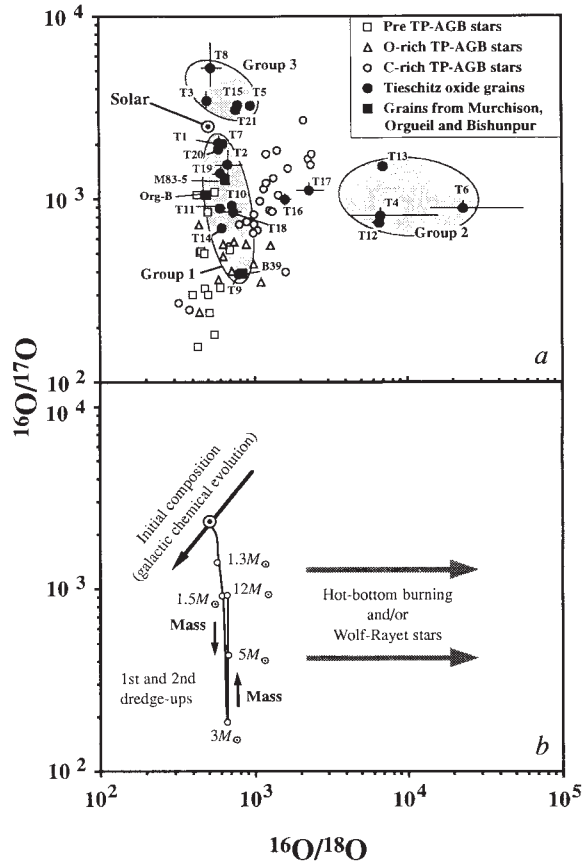

FIG. 1 *a*, Comparison of the oxygen isotope compositions of 24 interstellar oxide grains reported here and elsewhere[3–7] with those of red giant stars[13,14,20,21]. The red giant stars in *a* have been divided into three groups based on their spectral types and models of their evolution[15]. The oxide grains have also been divided into three groups based on their oxygen isotope compositions. *b*, Diagram of the expected oxgyen isotope compositions of red giant envelopes after the first and second dredge-ups as a function of stellar mass and initial composition. After core H-burning ceases, ^{17}O-enriched H-burnt material from the interior is mixed into the O-rich envelope of a red giant during two dredge-up episodes[15] (the second only in $>5M_\odot$ stars). The curve shows the predicted post-dredge-up ratios of stars with initially solar compositions but different masses[18]. The initial $^{16}O/^{17}O$ ratio influences the final ratio only in (1–1.5)$M_\odot$ stars[17]. The $^{16}O/^{18}O$ ratio is only slightly affected by these two dredge-ups[17]. The range of $^{16}O/^{17}O$ and $^{16}O/^{18}O$ ratios amongst Group 1 grains suggests that they come from several stars with different masses and different initial compositions. The initial oxygen isotope compositions, reflecting Galactic evolution, probably varied roughy as indicated (F. Timmes, personal communication). Subsequently, during the thermally pulsing asymptotic giant branch (TP-AGB) phase a third multiple dredge-up episode brings ^{12}C-rich He-burnt material to the surface. As a result, (1–5)$M_\odot$ stars will eventually become carbon stars (C/O > 1), but for (5–8)$M_\odot$ stars, H-burning at the base of the envelope (hot-bottom burning) is predicted to destroy ^{12}C and ^{18}O, thereby preventing formation of a carbon star[31]. Note that oxide grains may form even in carbon-star envelopes[32].

The third dredge-up is expected to bring to the star's surface ^{26}Al that was produced by shell H-burning at much higher temperatures than those reached during core H-burning[22,23]. Models predict envelope $^{26}Al/^{27}Al$ ratios in the range from 5×10^{-4} to 10^{-2}, depending on stellar mass, mass loss rate and evolutionary stage during the TP-AGB phase. Eight of the ten Group 1 grains measured for Al-Mg have inferred initial $^{26}Al/^{27}Al$ ratios in this range (Fig. 2). An alternative production mechanism for ^{26}Al is H-burning at the base of the convective envelope of TP-AGB

TABLE 1 Isotopic compositions of 24 meteoritic interstellar oxide grains

Grain	$^{17}O/^{16}O$	$^{18}O/^{16}O$	$^{26}Mg^*/^{24}Mg$	$^{27}Al/^{24}Mg$	$^{26}Al/^{27}Al$	Group
Solar	3.83×10^{-4}	2.01×10^{-3}				
T1	$5.01\,(39)\times10^{-4}$	$1.66\,(12)\times10^{-3}$	≤0.033	209 (32)	$\leq1.6\times10^{-4}$	1
T2	$6.6\,(1.1)\times10^{-4}$	$1.44\,(27)\times10^{-3}$	2.04 (19)	263 (65)	$7.8\,(2.0)\times10^{-3}$	1
T7	$5.05\,(22)\times10^{-4}$	$1.55\,(7)\times10^{-3}$	0.369 (15)	139 (18)	$2.65\,(37)\times10^{-3}$	1
T9	$2.63\,(5)\times10^{-3}$	$1.27\,(5)\times10^{-3}$	0.586 (83)	1086 (98)	$5.40\,(90)\times10^{-4}$	1
T10	$1.11\,(3)\times10^{-3}$	$1.36\,(6)\times10^{-3}$	≤0.042	402 (37)	$\leq1.0\times10^{-4}$	1
T11	$1.14\,(5)\times10^{-3}$	$1.60\,(10)\times10^{-3}$	NA	NA	NA	1
T14	$1.47\,(5)\times10^{-3}$	$1.57\,(9)\times10^{-3}$	0.163 (81)	1351 (271)	$1.20\,(64)\times10^{-4}$	1
T18	$1.19\,(8)\times10^{-3}$	$1.35\,(15)\times10^{-3}$	NA	NA	NA	1
T19	$7.50\,(74)\times10^{-4}$	$1.63\,(19)\times10^{-3}$	NA	NA	NA	1
T20	$5.38\,(16)\times10^{-4}$	$1.66\,(47)\times10^{-3}$	0.0303 (14)	41 (2)	$7.34\,(46)\times10^{-4}$	1
M83-5	$7.92\,(23)\times10^{-4}$	$1.52\,(5)\times10^{-3}$	1.96 (11)	2250 (109)	$8.73\,(64)\times10^{-4}$	1
Org-B	$9.72\,(10)\times10^{-4}$	$1.99\,(4)\times10^{-3}$	1.61 (3)	1840 (90)	$8.7\,(1)\times10^{-4}$	1
B39	$2.60\,(6)\times10^{-3}$	$1.17\,(4)\times10^{-3}$	0.2336 (104)	136 (14)	$1.7\,(0.2)\times10^{-3}$	1
T16	$1.01\,(6)\times10^{-3}$	$6.21\,(54)\times10^{-4}$	NA	NA	NA	1/2
T17	$9.12\,(76)\times10^{-4}$	$4.30\,(89)\times10^{-4}$	NA	NA	NA	1/2
T4	$1.26\,(11)\times10^{-3}$	$1.47\,(85)\times10^{-4}$	0.064 (13)	17.0 (2.3)	$3.77\,(91)\times10^{-3}$	2
T6	$1.14\,(8)\times10^{-3}$	$4.3\,(2.6)\times10^{-5}$	0.423 (57)	106 (16)	$4.01\,(82)\times10^{-3}$	2
T12	$1.36\,(4)\times10^{-3}$	$1.50\,(11)\times10^{-4}$	0.969 (81)	135 (11)	$7.19\,(83)\times10^{-3}$	2
T13	$6.72\,(24)\times10^{-4}$	$1.41\,(10)\times10^{-4}$	10.4 (13)	5442 (707)	$1.90\,(35)\times10^{-3}$	2
T3	$2.92\,(29)\times10^{-4}$	$1.98\,(13)\times10^{-3}$	≤0.0048	8.2 (1)	$\leq6.0\times10^{-4}$	3
T5	$3.15\,(11)\times10^{-4}$	$1.02\,(3)\times10^{-3}$	≤0.0099	47 (6)	$\leq2.1\times10^{-4}$	3
T8	$1.92\,(51)\times10^{-4}$	$1.85\,(29)\times10^{-3}$	NA	NA	NA	3
T15	$3.20\,(23)\times10^{-4}$	$1.26\,(6)\times10^{-3}$	NA	NA	NA	3
T21	$3.25\,(17)\times10^{-4}$	$1.29\,(59)\times10^{-3}$	≤0.025	549 (33)	$\leq4.6\times10^{-5}$	3

The (meteorite) source of the grains is shown in the first column; Tieschitz (T), Murchison (M)[4], Orgueil (Org)[3,5,6] and Bishunpur (B)[7]. The grains have been divided into three groups on the basis of their oxygen isotopic compositions. $^{26}Mg^*$ is the excess of ^{26}Mg after correction for mass fractionation, and $^{26}Al/^{27}Al$ is the initial ratio if all $^{26}Mg^*$ results from the *in situ* decay of ^{26}Al. All errors, in parenthesis, are 1σ and upper limits are 2σ. All grains were analysed by SEM-EDS (Scanning electron microscopy—energy dispersive spectroscopy) after oxygen isotope measurements but before Mg-Al analysis in the ion probe. All but grain T3 appear to be corundum (Al_2O_3). The Al/Mg ratio of grain T3, measured by EDS, is about twice that expected for pure spinel ($MgAl_2O_4$) but much lower than those of the other grains. The ratio obtained in the subsequent ion-probe analysis of T3 is even higher, suggesting that the grain may be an intergrowth of spinel and corundum. The oxygen isotope ratios are given with ^{16}O in the denominator because in the reverse case the errors are asymmetric and nonlinear.

stars of $>5M_\odot$ (hot-bottom burning)[24,25]. But during hot-bottom burning the whole envelope is cycled through the high-temperature H-burning zone, resulting in the destruction of essentially all ^{18}O (producing high $^{16}O/^{18}O$ ratios), in disagreement with the oxygen isotope ratios observed in Group 1 grains. The oxygen isotope and $^{26}Al/^{27}Al$ ratios of these grains thus indicate that at least eight of them come from TP-AGB stars, and at least two from red giants before they reached the TP-AGB phase. It is worth noting that whereas the oxygen isotopes in red giant envelopes can be measured astronomically—albeit with larger errors than those obtained in the grains—the determination of $^{26}Al/^{27}Al$ ratios in such stars is only possible from the laboratory analysis of pre-solar grains.

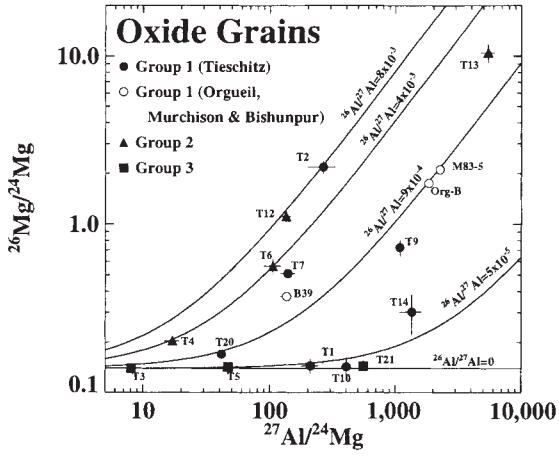

FIG. 2 Plot of the $^{26}Mg/^{24}Mg$ ratio versus the $^{27}Al/^{24}Mg$ ratio in 17 pre-solar oxide grains. The large ^{26}Mg excesses, compared to solar Mg isotopic ratios, are best explained as the result of *in situ* decay of ^{26}Al. Also shown are Al-Mg evolution lines for five initial $^{26}Al/^{27}Al$ ratios. The $^{27}Al/^{24}Mg$ ratios in most of the Tieschitz corundum grains are not as high as might be expected, possibly because of significant background contributions from isotopically normal Mg to the Mg analysis. However, these contributions do not affect the inferred $^{26}Al/^{27}Al$ ratios.

Unlike grains in Group 1, neither Group 2 nor Group 3 grains have spectroscopic counterparts and we must rely solely on comparisons with stellar evolution models to infer their likely sources. Group 2 grains have ^{17}O and ^{26}Al enrichments, and ^{18}O depletions that are much larger than previously observed in any meteoritic material or star. Two other grains, which lie on the edge of the carbon-star field, have intermediate ^{18}O depletions. Relatively low-temperature hot-bottom burning could destroy essentially all ^{18}O in an AGB envelope without significantly changing the ^{26}Al and ^{17}O abundances already established by the first, second and third dredge-ups[17]. Also, such isotopic compositions are predicted to exist at the surface of massive mass-losing stars which have shed their envelopes, exposing the H-burnt interior (Wolf–Rayet stars during the Of-WN phases)[26]. In any case, better modelling and more elemental and isotopic data on Group 2 grains are necessary for distinguishing between the two possible sources.

The Group 3 grains are moderately depleted in ^{17}O relative to the Solar System. They could conceivably have formed around low-mass red giant stars that have experienced the first dredge-up, provided that the initial $^{16}O/^{17}O$ ratios of the stars were higher than the measured grain values and, therefore, the solar value. On the other hand, massive stars ($>10\,M_\odot$), which contribute ~6–12% of all Galactic dust[8,9], produce large excesses of ^{16}O and ^{18}O in certain shells[27] that could come to the surface as the star loses mass or could be ejected in a supernova explosion.

^{16}O enrichments and depletions with respect to the terrestrial isotopic ratios are common in materials of Solar System origin[28]; in meteorites the enrichments can reach up to 7% in corundum (Al_2O_3) and spinel ($MgAl_2O_4$) from Ca-Al-rich inclusions[29]. These enrichments prompted suggestions that ^{16}O-rich grains, probably corundum and spinel, from a supernova were incompletely mixed into the Solar System[28]. We have not found any

pre-solar grains with large ^{16}O enrichments. The Group 3 grains are ^{16}O-rich, but not with respect to both ^{17}O and ^{18}O. The discovery that ^{16}O can undergo mass-independent gas-phase chemical fractionation from both ^{17}O and ^{18}O has provided an alternative explanation for the observed ^{16}O enrichments in Solar System material[30].

Finally, if the Si/Al ratio is assumed to be solar in all stars and if all Al goes into corundum (Al_2O_3), interstellar corundum appears to be underabundant in meteorites, relative to interstellar SiC, by about a factor of between 20 and 50 (refs 4, 6, 10) when compaerd to estimated Galactic dust production rates[8,9]. This is in spite of the fact that, in the solar nebula, corundum should have been more stable than SiC. Possible explanations are that interstellar corundum has a finer grain size distribution than SiC and was thus not detected by our technique, that Al primarily condenses in other phases (such as silicates) that are less resistant to the chemical treatments used to isolate the grains or, most speculatively, that corundum has a shorter lifetime in the interstellar medium than SiC. □

Received 25 February; accepted 28 June 1994.

1. Anders, E. & Zinner, E. K. *Meteoritics* **28,** 490–514 (1993).
2. Ott, U. *Nature* **364,** 25–33 (1993).
3. Huss, G. R., Hutcheon, I. D., Wasserburg, G. J. & Stone, J. *Lunar planet. Sci.* **XXIII,** 563–564 (1992).
4. Nittler, L. R., Walker, R. M., Zinner, E. K., Hoppe, P. & Lewis, R. S. *Lunar planet. Sci.* **XXIV,** 1087–1088 (1993).
5. Huss, G. R., Hutcheon, I. D., Fahey, A. J. & Wasserburg, G. J. *Meteoritics* **28,** 369–370 (1993).
6. Hutcheon, I. D., Huss, G. R., Fahey, A. J. & Wasserburg, G. J. *Astrophys. J.* **425,** L97–L100 (1994).
7. Huss, G. R., Fahey, A. J., Gallino, R. & Wasserburg, G. J. *Astrophys. J.* (in the press).
8. Gehrz, R. D. in *Interstellar Dust* (eds Allamandola, L. J. & Tielens, A. G. G.) 445–453 (Kluwer Academic, Dordrecht, 1989).
9. Whittet, D. C. B. *Dust in the Galactic Environment*, 295 (Institute of Physics, Bristol, 1992).
10. Nittler, L. R., Alexander, C. M. O'D., Gao, X., Walker, R. M & Zinner, E. K. *Lunar planet. Sci.* **XXV,** 1005–1006 (1994).
11. Gao, X., Alexander, C. M. O'D., Swan, P. D. & Walker, R. M. *Lunar planet. Sci.* **XXV,** 401–402 (1994).
12. Zinner, E. K., Tang, M. & Anders, E. *Geochim. cosmochim. Acta* **53,** 3273–3290 (1989).
13. Harris, M. J. & Lambert, D. L. *Astrophys. J.* **285,** 674–682 (1984).
14. Smith, V. V. & Lambert, D. L. *Astrophys. J. Suppl. Ser.* **72,** 387–416 (1990).
15. Iben, I. Jr. *Astrophys. J. Suppl. Ser.* **76,** 55–114 (1991).
16. Dearborn, D. S. P. *Phys. Rep.* **210,** 367–382 (1992).
17. Boothroyd, A. I., Sackmann, I. J. & Wasserburg, G. J. *Astrophys. J.* (in the press).
18. El Eid, M. F. *Astr. Astrophys.* **285,** 915–928 (1994).
19. Edvardsson, B. *et al. Astr. Astrophys.* **275,** 101–152 (1993).
20. Harris, M. J., Lambert, D. L., Hinkle, K. H., Gustafsson, B. & Eriksson, K. *Astrophys. J.* **316,** 294–304 (1987).
21. Kahane, C., Cernicharo, J., Gomez-Gonzalez, J. & Guelin, M. *Astr. Astrophys.* **256,** 235–250 (1992).
22. Forestini, M., Paulus, G. & Arnould, M. *Astr. Astrophys.* **252,** 597–604 (1991).
23. Gallino, R., Raiteri, C. M., Busso, M. & Matteucci, F. *Astrophys. J.* (in the press).
24. Nørgaard, H. *Astrophys. J.* **236,** 895–898 (1980).
25. Cameron, A. G. W. in *Protostars and Planets III* (eds Levy, E. H. & Lunine, J. I.) 47–73 (Univ. Arizona Press, 1993).
26. Prantzos, N., Doom, C., Arnould, M. & de Loore, C. *Astrophys. J.* **304,** 695–712 (1986).
27. Woosley, S. E. in *Nucleosynthesis and Chemical Evolution* (eds Hauck, B., Maeder, A. & Meynet, G.) 1–195 (Observatoire de Genève, Geneva, 1986).
28. Clayton, R. N., Grossman, L. & Mayeda, T. K. *Science* **182,** 485–488 (1973).
29. Virag, A., Zinner, E. K., Amari, S. & Anders, E. *Geochim. Cosmochim. Acta* **55,** 2045–2062 (1991).
30. Thiemens, M. H. & Heidenreich, J. E. *Science* **219,** 1073–1075 (1983).
31. Renzini, A. & Voli, M. *Astr. Astrophys.* **94,** 175–193 (1981).
32. Lattimer, J. M., Schramm, D. N. & Grossman, L. *Astrophys. J.* **219,** 230–249 (1978).

ACKNOWLEDGEMENTS. We thank G. Huss and A. G. W. Cameron for their constructive reviews. This work was supported by NASA.

Directional motion of brownian particles induced by a periodic asymmetric potential

Juliette Rousselet*, Laurence Salome*, Armand Ajdari† & Jacques Prost†

* Centre de Recherche Paul Pascal, Avenue A. Schweitzer, 33600 Pessac, France
† Groupe de Physico Chimie Théorique, URA 1382 CNRS, E.S.P.C.I., 10, rue Vauquelin, 75231 Paris Cédex 05, France

STRUCTURES possessing spatial asymmetry should act as pumps in the presence of dissipation alone[1–4], without the need for macroscopic forces or temperature differences[5] to drive vectorial motion. It has been shown theoretically[2–4,6,7] that particles subjected to an asymmetric periodic potential can display net directional motion even if the space-averaged force is zero. Here we demonstrate such behaviour experimentally. We have studied the behaviour of colloidal particles suspended in solution and exposed to a sawtooth dielectric potential which is turned on and off periodically. The particles exhibit net motion with a velocity that depends on their size, suggesting applications in separation processes for objects in the size range 0.1–5 μm—a range that includes biological structures such as viruses, cells and chromosomes[8]. We furthermore point out the analogy between our device and motor protein assemblies.

Consider an asymmetric potential U_{on} applied periodically for a period τ_{on} and then switched off for a period τ_{off} (Fig. 1*A*). At the end of an 'on' period, the particles are trapped in the minima of the potential U_{on}, so that the concentration of particles is peaked around the corresponding positions (Fig. 1*B*). During the following 'off' period the particles diffuse freely so that the concentration at the end of this 'off' period is a set of gaussian curves centred around the same points (Fig. 1*C*). Turning the potential on again will induce 'downhill' motion of particles (Fig. 1*A*). The result of this off–on cycle is that the particles corresponding to the hatched areas move to the right, whereas essentially none move to the left. In a more general picture a proportion $P(m)$ would make an m-step progression, with $P(m) > P(-m)$ owing to the asymmetry. The result is to achieve macroscopic drift in a single direction.

In our experiments, colloidal particles were confined between two glass slides and subjected to a spatially asymmetric and periodic a.c. electric field E, which was successively turned on and off. The field was generated by interdigitated electrode deposited on one of the glass slides with standard photolithographic techniques (Innovations Couches Minces Co., Le Coudray Montceaux, France), the shape of which provided the necessary asymmetry (Fig. 2). The 'Christmas tree' design was chosen in such a way that the dielectric energy profile $(-\frac{1}{2}\Delta\alpha E^2$; where $\Delta\alpha$ is the polarizability of the particle relative to the suspending solution) along a line between two adjacent electrodes, was similar to that in Fig. 1, with a 50-μm period. The neck width between two adjacent electrodes was 5 μm, giving fields as high as 2×10^4 V cm^{-1} for applied voltages of just 10 V.

Experiments were performed on functionalized polystyrene latex spheres of diameter 0.25 μm, 0.4 μm (fluorescent particles provided by Molecular Probes, Eugene, Oregon) and 1 μm (provided by Interchim, Montluçon, France). The particles were suspended solution (tris (tris(hydroxymethyl)aminomethane) 44.5 mM, boric acid 44.5 mM, EDTA (ethylenediaminetetraacetic acid) 1.2 mM, in water), promoting substantial dissociation of the carboxylate groups at their surface. These conditions were prefered to 'pure' water both because of the easy control of the solution, and its wide use in biological systems. Electrodes were not protected by a passivation layer, and in order to avoid electrolysis a.c. voltages with frequencies higher than 500 Hz were applied. The particle diameters were measured by light-scattering techniques and found to be within 10% of the specifications; their diffusion constants were measured from direct observation of the brownian motion between glass slides, and found to agree with the Stokes–Einstein formula within 15% (diffusion close to the walls is discussed in a preprint by L. Faucheux and A. Libchaber, NEC Research Institute, Princeton NJ). Their dielectrophoretic response was also studied independently, and revealed